Tetrisation of Triangular Meshes and Its Application in Shape Blending

Shizuo Kaji

Abstract The As-Rigid-As-Possible (ARAP) shape deformation framework is a versatile technique for morphing, surface modelling, and mesh editing. We discuss an improvement of the ARAP framework in a few aspects: 1. Given a triangular mesh in 3D space, we introduce a method to associate a tetrahedral structure, which encodes the geometry of the original mesh. 2. We use a Lie algebra based method to interpolate local transformation, which provides better handling of rotation with large angle. 3. We propose a new error function to compile local transformations into a global piecewise linear map, which is rotation invariant and easy to minimise. We implemented a shape blender based on our algorithm and its MIT licensed source code is available online.

Keywords Shape blending · Tetrahedral mesh · As-rigid-as-possible deformation

1 Introduction

In Shape blending the seminal paper [1], they introduced a morphing algorithm called the As-Rigid-As-Possible (ARAP, for short) shape interpolation. Since then, the technique has been successfully applied to various shape deformation applications. In their original paper, tetrahedral volume meshes are used to produce interpolation of shapes. However, in most computer graphic systems it is common to represent shapes by surface meshes. To convert a surface mesh to a volume mesh is a non-trivial task (see, for example, [13]) and the resulting volume mesh tends to have many extra internal vertices, which makes applications inefficient. Instead of considering volume meshes, one can "fatten" surface meshes. A common practice is to associate a tetrahedral structure to a triangular surface mesh by adding the normal vector for every triangle (see, for example, [15]). Although this simple trick has been widely

S. Kaji (✉)
Yamaguchi University/JST CREST, 1677-1, Yoshida, Yamaguchi 753-8512, Japan
e-mail: skaji@yamaguchi-u.ac.jp

Y. Dobashi and H. Ochiai (eds.), *Mathematical Progress in Expressive Image Synthesis III*, Mathematics for Industry 24,
DOI 10.1007/978-981-10-1076-7_2

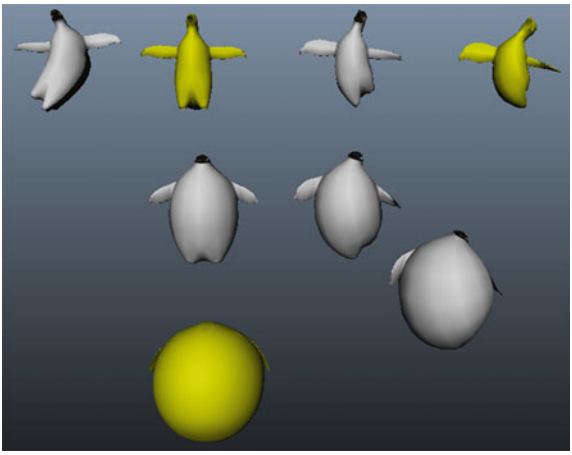

Fig. 1 Three shapes (*yellow*) are blended to produce variations (*white*). Not only interpolation but also extrapolation (with weights >1 or <0) is possible. The *top-left shape* is obtained by extrapolating the two *yellow shapes* in the *top row*

used, it does not capture important geometric features of the mesh. For example, the relation between adjacent triangles is neglected.

One of the main purposes of this paper is to introduce a new construction to associate a tetrahedral structure to a triangular mesh, which we call *tetrisation* (Sect. 4). Our method encodes inter-triangular properties such as the angle between adjacent triangles so that one can keep track of global geometry such as curvature while working locally on tetrahedra.

We also discuss an improvement of the ARAP (Sect. 3) in how to interpolate local transformations (Sect. 5) and how to stitch fragmented tetrahedra by a new error function (Sect. 6). We demonstrate our improvement by a shape blending application (Fig. 1). Given an arbitrary number of isomorphic surfaces, our algorithm produces inter/extrapolation of the shapes according to the weights given by the user. Roughly speaking, we define a "linear combination" of shapes

$$w_1 Q_1 + w_2 Q_2 + \cdots + w_m Q_m,$$

where $w_i \in \mathbb{R}$ are weights and Q_i are shapes. In particular, when the number of shapes is two, $w_1 Q_1 + (1 - w_1) Q_2$ for $0 \leq w_1 \leq 1$ gives a morphing between them. Note that our algorithm is highly non-linear although we described the procedure as taking the linear combination of shapes. We implemented the algorithm as the Autodesk Maya plugin. Its MIT licensed source code is available at [6].

2 Notation

We begin with listing some notation. We assume all transformations are represented by real matrices, acting on real column vectors by the multiplication from the left.

- SO(3): the group of 3D rotations. Its element is a 3×3 special orthogonal matrix.
- $\mathrm{Sym}^+(3)$: the set of 3D shears. Its element is a 3×3 positive definite symmetric matrix.
- GL(3): the group of (invertible) 3D linear transformations consisting of compositions of rotation, shear, and reflection. Its element is a 3×3 regular matrix.
- Aff(3): the group of (invertible) 3D affine transformations consisting of compositions of rotation, shear, reflection, and translation. Its element is a 4×4 regular homogeneous matrix.
- $\mathrm{GL}^+(3)$, $\mathrm{Aff}^+(3)$: the subgroups of the reflection free (positive determinant) elements in the corresponding groups.
- $\hat{A} \in \mathrm{GL}(3)$: the linear part ($3 \times 3$ upper-left corner) of $A \in \mathrm{Aff}(3)$.
- A^t: the transpose of a matrix A.
- $|A|_F^2 = \mathrm{tr}(A^t A)$: the squared Frobenius norm of a matrix A.
- $\#U$: the cardinality of a set U.

3 As-Rigid-As-Possible Deformation Framework

In this section, we recall the ARAP framework by describing an algorithm for shape blending. Note that although we discuss shape blending as the primary application, the framework and our improvement is not limited to it. Indeed, after being introduced in [1] initially as a morphing algorithm, the ARAP technique has been serving as one of the fundamental frameworks for various kinds of shape deformation applications (see, for example, [3, 7, 14–16]).

Our problem setting is as follows. We are given a rest shape V_0 and m its deformations V_j ($1 \le j \le m$). That is, a vertex correspondence between V_0 and each of V_j ($1 \le j \le m$) is assumed. We would like to compute the deformation $V(w_1, \ldots, w_m)$ by blending the given shapes $\{V_j\}$ according to the user specified weights $\{w_j \in \mathbb{R} \mid 1 \le j \le m\}$. We insist that it interpolates the given shapes, i.e., $V(0, \ldots, 0) = V_0$, and $V(w_1, \ldots, w_m) = V_k$ when $w_j = \begin{cases} 1 & (j = k) \\ 0 & (j \neq k) \end{cases}$. Notice we allow negative weights and weights greater than one so that the system can not only interpolate but also extrapolate.

Remark 1 A basic shape blending is achieved by simply taking the linear combination of the coordinates of the vertices. This method is very fast and widely used to produce variations of shapes, in particular, facial expressions. However, since the geometry of shapes is disregarded, it does not always produce plausible outputs (Fig. 2). The ARAP based method which we will describe below takes geometry into account to obtain better results.

We assume that the rest shape is equipped with a non-degenerate *tetrahedral structure* $(V_0, \mathscr{T})$. We will discuss in Sect. 4 a method to associate one to a triangular mesh.

Fig. 2 Interpolation between *yellow shapes*. *Left* linear method. *Right* our method

Definition 1 A tetrahedral structure is a pair $(V, \mathscr{T})$, where the vertex set V consists of three dimensional vectors and the set of tetrahedra $\mathscr{T} = \{T_i \mid 1 \le i \le n\}$ consists of ordered tuples of four distinct vertices $T_i = (v_{i_1}, v_{i_2}, v_{i_3}, v_{i_4})$. Each vertex in V must be contained in at least one tetrahedron. A tetrahedral structure is said to be non-degenerate when the vertices of each tetrahedron are not co-planar.

We emphasise that a triangle can be shared by three or more tetrahedra, and for this reason, we use the terminology "tetrahedral structure" rather than tetrahedral mesh.

The information of a tetrahedral structure $(V, \mathscr{T})$ can be packed into a collection of 4×4-matrices:

$$\left\{ P_i := \begin{pmatrix} v_{i_1}(x) & v_{i_2}(x) & v_{i_3}(x) & v_{i_4}(x) \\ v_{i_1}(y) & v_{i_2}(y) & v_{i_3}(y) & v_{i_4}(y) \\ v_{i_1}(z) & v_{i_2}(z) & v_{i_3}(z) & v_{i_4}(z) \\ 1 & 1 & 1 & 1 \end{pmatrix} \middle| 1 \le i \le n \right\}, \tag{1}$$

where $(v_{i_j}(x), v_{i_j}(y), v_{i_j}(z))^t \in \mathbb{R}^3$ is the vector representing the position of the vertex $v_{i_j} \in V$.

We denote by $\{P_{0i} \mid 1 \le i \le n\}$ the matrices associated to the rest shape $(V_0, \mathscr{T})$. Since $(V_0, \mathscr{T})$ is assumed to be non-degenerate, all the P_{0i} are regular. For each deformation V_j, we use the same set of tetrahedra $\mathscr{T}$ to obtain $\{P_{ji} \mid 1 \le i \le n\}$. Note that P_{ji} need not be regular. We define a series of affine transformations

$$A_{ji} := P_{ji} P_{0i}^{-1} \ (1 \le i \le n) \tag{2}$$

which maps the vertices V_0 of the rest shape to the ones V_j in the deformed shape. Obviously, $A_{ji}v = A_{ji'}v$ when $v \in V_0$ is contained in two tetrahedra T_i and $T_{i'}$. Thus, $\{P_{ji} \mid 1 \le i \le n\}$ can be considered as a *piecewise linear map* defined on $(V_0, \mathscr{T})$ with $(V_j, \mathscr{T})$ as its image.

Now, we have m piecewise linear maps $\left\{P_{ji} \mid 1 \le i \le n\right\}_{j=1}^{m}$ and the problem is rephrased as to blend them according to the user specified weights w_j $(1 \le j \le m)$. We first consider locally and blend $\hat{P}_{ji}$ $(1 \le j \le m)$ for a single tetrahedron T_i to obtain $C_i \in \mathrm{GL}^+(3)$. Intuitively, C_i stipulates the local transformation for the tetrahedron T_i. We discuss a method to compute C_i in Sect. 5. The last step is to find a global piecewise linear map on $(V_0, \mathscr{T})$, whose image we take as the output. Since we cannot assume $C_i v$ agrees with $C_{i'} v$ for a vertex $v \in V_0$ which is contained in two tetrahedra T_i and $T_{i'}$, we have to "stitch" them. What we do is to find a piecewise

linear map which is closest to the collection $\{C_i \mid 1 \leq i \leq n\}$ with respect to an *error function*. We discuss different error functions in Sect. 6. The deformed shape $V(w_1, \ldots, w_m)$ is computed as the minimiser of the error function.

In the following sections, we discuss each step in detail.

4 Tetrisation

In computer graphics systems, shapes are usually represented by surface meshes. To apply the ARAP technique described in the previous section, we have to have a tetrahedral structure. Here, we consider a method to build a tetrahedral structure from a given triangular surface mesh.

Definition 2 For a triangular mesh, we denote an element of the vertex set V by a three dimensional vector and an element of the set of (face) triangles $\mathscr{F}$ by an ordered tuple of three vertices (v_1, v_2, v_3). For $(v_1, v_2, v_3) \in \mathscr{F}$, we call the ordered tuples v_1v_2, v_2v_3 and v_3v_1 the *oriented edges*. A triangular mesh is said to be *non-degenerate* when the vertices of each triangle are not co-linear.

Given a triangular mesh, we would like to associate a tetrahedral structure which we can apply the ARAP framework to.

Definition 3 Given a non-degenerate triangular mesh $(V, \mathscr{F})$. A *tetrisation* of $(V, \mathscr{F})$ is a tetrahedral structure which consists of the vertex set $\bar{V}$ and the set of tetrahedra $\mathscr{T}$. We require $(\bar{V}, \mathscr{T})$ to satisfy the following conditions:

1. $V \subset \bar{V}$. That is, $\bar{V}$ is obtained by adding *ghost vertices* to V.
2. Each triangle in $\mathscr{F}$ has to be contained in at least one tetrahedron in $\mathscr{T}$.
3. Each tetrahedron is non-degenerate, that is, the four vertices are not co-planar.

These conditions are exactly what are required in the ARAP framework.

We give three methods to produce tetrisation in the following. Recall that the unit normal vector $n(F)$ of a triangle $F = (v_1, v_2, v_3)$ is computed by $\dfrac{(v_2 - v_1) \times (v_3 - v_1)}{|(v_2 - v_1) \times (v_3 - v_1)|}$, where the denominator $|(v_2 - v_1) \times (v_3 - v_1)|$ is twice the area $2\mathrm{Area}(F)$ of F.

4.1 Face-Normal Tetrisation

We begin with a simple method which has been commonly used in various applications. For each triangle $F = (v_1, v_2, v_3)$ in $\mathscr{F}$, add the ghost vertex

$$v_0 = \frac{(v_1 + v_2 + v_3)}{3} + \frac{(v_2 - v_1) \times (v_3 - v_1)}{\sqrt{|(v_2 - v_1) \times (v_3 - v_1)|}}$$

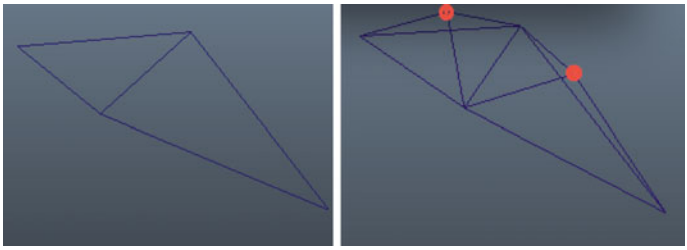

Fig. 3 *Left* the original surface. *Right* its face-normal tetrisation. Ghost vertices are marked with a *red circle*

and form a tetrahedron (v_0, v_1, v_2, v_3). The resulting tetrahedral structure has $\#\mathscr{T} = \#\mathscr{F}$ and $\#\bar{V} = \#V + \#\mathscr{T}$.

A problem with this tetrisation when applied to the ARAP framework is that this does not capture the relation between adjacent triangles. For example, consider two triangles sharing an edge as in Fig. 3. Any rotation invariant error function (see Sect. 6) with $C_1 = C_2 = Id$ will be minimised regardless of the angle between the two triangles. In other words, folds do not cause any penalty in the error function.

4.2 Edge-Normal Tetrisation

We assume each oriented edge appears only once among all the triangles. In other words, an unoriented edge should be contained at most two triangles with opposite orientations. Also, we assume all the triangles have at least one shared edge, that is, there is no "lone" triangle. (We can remove this assumption by adding ghost vertices not only for shared edges but also for all edges. However, this is inefficient and makes no sense.)

For each shared edge v_1v_2, denote by $F_1 = (v_1, v_2, v_3)$ and $F_2 = (v_1, v_4, v_2)$ the two triangles adjacent to it. Add a ghost vertex

$$v_0 = \frac{v_1 + v_2}{2} + |v_1 - v_2| \frac{n(F_1) + n(F_2)}{|n(F_1) + n(F_2)|}$$

and form two tetrahedra (v_0, v_1, v_2, v_3) and (v_0, v_1, v_4, v_2). The resulting tetrahedral structure (Fig. 4) has $\#\mathscr{T} = 2 \cdot \#(\text{shared edges})$ and $\#\bar{V} = \#V + \#(\text{shared edges})$. The idea of this tetrisation is to encode the angle between adjacent triangles, which is neglected by the face-normal tetrisation.

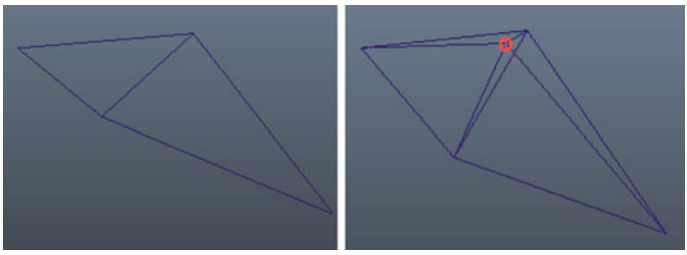

Fig. 4 *Left* the original surface. *Right* its edge-normal tetrisation. Ghost vertex is marked with a *red circle*

4.3 Vertex-Normal Tetrisation

We assume that every vertex has a neighbourhood homeomorphic to the plane or the half plane. In other words, the mesh is a manifold (with boundary). Also, we assume all the triangles have at least one shared vertex. (Again, we can remove this assumption as in the previous subsection.)

For each shared vertex v, denote the adjacent triangles by $F_1, F_2, \ldots,$ and F_k. Add a ghost vertex

$$v_0 = v + \sqrt{\sum_{i=1}^{k} \mathrm{Area}(F_i)} \frac{n(F_1) + \cdots + n(F_k)}{|n(F_1) + \cdots + n(F_k)|}$$

and form k tetrahedra by adding v_0 to the triangles F_i $(1 \leq i \leq k)$. The resulting tetrahedral structure (Fig. 5) has $\#\mathscr{T} = 3\#\mathscr{F} - \#(\text{non-shared vertices})$ and $\#\bar{V} = \#V + \#(\text{shared vertices})$. An advantage of this method is that it extends straightforwardly to general polyhedral meshes. The idea of this tetrisation is to encode the angle around internal vertices, which is neglected by the face-normal tetrisation.

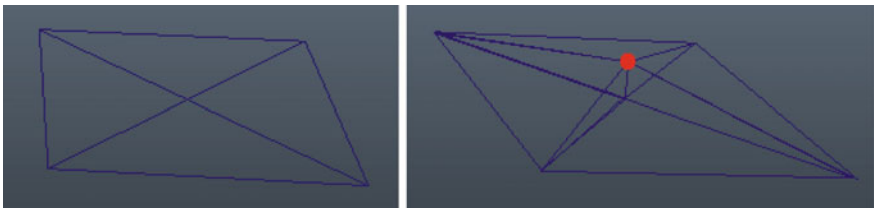

Fig. 5 *Left* the original surface. *Right* its vertex-normal tetrisation. Ghost vertex is marked with a *red circle*. Ghost vertices on the boundary are omitted for simplicity

5 Blending Linear Maps

In this section, we discuss how to blend local transformations $\hat{A}_{1i}, \hat{A}_{2i}, \dots, \hat{A}_{mi} \in \mathrm{GL}^+(3)$ with regard to the weights $w_1, \dots, w_m \in \mathbb{R}$ to obtain the blended local transformation $C_i \in \mathrm{GL}^+(3)$. For this purpose, we use a function $\mathrm{Blend} : \mathbb{R}^m \times (\mathrm{GL}^+(3))^m \to \mathrm{GL}^+(3)$ which satisfies the obvious requirement for interpolation. Then, we set

$$C_i := \mathrm{Blend}(w_1, \dots, w_m, \hat{A}_{1i}, \hat{A}_{2i}, \dots, \hat{A}_{mi}).$$

We investigate two such interpolation functions.

First, decompose each $\hat{A}_{ki}$ by the polar decomposition (see, for example, [5, 12])

$$\hat{A}_{ki} = R_{ki} S_{ki}$$

where $R_{ki} \in \mathrm{SO}(3)$ is the rotation and $S_{ki} \in \mathrm{Sym}^+(3)$ is the shear. In [16], they suggest

$$\mathrm{Blend}_P(w_1, \dots, w_m, \hat{A}_{1i}, \dots, \hat{A}_{mi}) = \exp\left(\sum_{k=1}^m w_k \log(R_{ki})\right)\left(\sum_{k=1}^m w_k S_{ki} + \left(1 - \sum_{k=1}^m w_k\right) I\right),$$

where log is the principal matrix logarithm and I is the identity matrix.[1] This coincides with the one used in [1] when $m = 1$. On the other hand, we suggest

$$\mathrm{Blend}_C(w_1, \dots, w_m, \hat{A}_{1i}, \dots, \hat{A}_{mi}) = \exp\left(\sum_{k=1}^m w_k \log^c(R_{ki})\right) \exp\left(\sum_{k=1}^m w_k \log(S_{ki})\right), \tag{3}$$

where $\log^c$ is the "continuous" logarithm such that it chooses the nearest branch of logarithm to the adjacent tetrahedra when i varies (see [8] for details). The indeterminacy of log for SO(3) is in the rotation angle and $\log^c$ chooses the angle continuously for adjacent tetrahedra. Note that [8] provides a direct and fast formula for Blend_C which does not require the polar decomposition.

They look similar but there are two significant differences; blending for the shear part and logarithm for SO(3). The value of Blend_P can fall out of $\mathrm{GL}^+(3)$ due to the linear blending of the shear part, which causes distortion in the output (Fig. 6). The use of the continuous logarithm enables the system to produce a smoother morph among shapes which performs large rotation in between (Fig. 7). Note that in [1] which discusses morphing of two shapes, they suggest to use the quaternions and SLERP ([11]) to interpolate the rotation part and the linear interpolation for the shear part. (With three or more shapes, one can use the linear blending of the quaternions for the rotation part as in [9].) However, this method shows similar deficiency as Blend_P.

[1] The term involving I is for normalisation and it enforces $\mathrm{Blend}_P(0, \dots, 0, \hat{A}_{1i}, \hat{A}_{2i}, \dots, \hat{A}_{mi}) = I$.

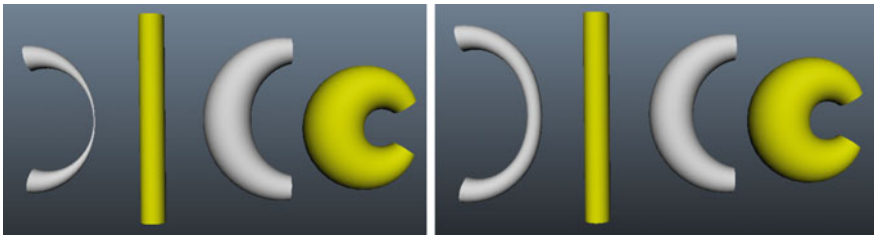

Fig. 6 Interpolation/extrapolation of *yellow shapes*. *Left* with Blend_P function in [16], the extrapolated shape on the *left* is degenerate. *Right* with our Blend_C function, the extrapolated shape is non-degenerate

Fig. 7 Interpolation of *yellow shapes*. *Left* with Blend_P function in [16], some parts try to rotate inconsistently. *Right* with our Blend_C function, local rotations are appropriately handled to produce a smooth interpolation

6 Error Function

In this section, we consider error functions to stitch fragmented tetrahedra. Fix the vertex positions V_0 of the rest shape and the local transformations $\{C_i \mid 1 \leq i \leq n\}$ of the tetrahedra. An error function is a function of the deformed vertex positions V'. By Eq. (2), a piecewise linear map $\{A_i \mid 1 \leq i \leq n\}$ and V' are linearly related and we identify them. In [1], they introduced

$$E_T(V', \{C_i\}) = \sum_{i=1}^{n} |\hat{A}_i - C_i|_F^2 \tag{4}$$

and it has been used in many of the ARAP based shape deformation applications including [2, 15–17]. Note that the function is translation invariant but not rotation invariant. Rotation invariance is sometimes preferable in shape deformation (see, for example, [10, 14] and Fig. 9). We propose an alternative error function which is rotation and translation invariant:

$$E_S(V', \{C_i\}) = \sum_{i=1}^{n} |S(\hat{A}_i) - S(C_i)|_F^2, \tag{5}$$

where $S(X)$ for $X \in \mathrm{GL}(3)$ is the shear factor of the polar decomposition of X (see [12]). Intuitively, this error function measures how much each tetrahedron is distorted. Despite the simplicity and its invariance property, E_S has not been considered in the literature as far as the author is aware. We believe this error function gives a good alternative to E_T in some applications (see Fig. 9).

Remark 2 We can assign a weight $W_i \in \mathbb{R}$ to each tetrahedron T_i to specify its contribution to the error function. It is done simply by replacing the summation $\sum_{i=1}^{n}$ with the weighted one $\sum_{i=1}^{n} W_i$ in the definitions of the error functions. For notational simplicity, we omit them in this paper.

As we described in Sect. 3, we define the output as the minimiser of the error function. In other words, we compute the piecewise linear function $\{A_i \mid 1 \le i \le n\}$ which is closest to $\{C_i \mid 1 \le i \le n\}$ with respect to the error function. Computing the minimiser for E_T is reduced to solving a sparse linear system (see [1, 16]). For E_S, the computation is not linear. An iterative way similar to [14] is given as follows:

1. Compute the minimiser of $E_T(V', \{C_i\})$ and set $\hat{A}_i$.
2. Compute the polar decomposition $\hat{A}_i = R_i S_i$.
3. Compute the minimiser of $E_T(V', \{R_i S(C_i)\})$ to update $\{\hat{A}_i\}$.
4. Repeat (2) and (3) until $\{\hat{A}_i\}$ converge.

Note that there is some indeterminacy of the minimiser coming from the symmetry of the error function. For example, any translation of a minimiser is also a minimiser. To obtain a unique minimiser, one can impose additional constraints; for E_T fixing the position of the barycentre and for E_S fixing the position of the barycentre and the orientation of some tetrahedra.

7 Implementation

We implemented our algorithm as the Autodesk Maya plugin [6]. In our system, the user can specify the weight for each shape with sliders, or the ball controller which computes the weights by [4] from the configuration of the balls representing the shapes (Fig. 8).

The ARAP framework was also applied to shape blending in [2] in the 2D setting and in [16] in the 3D setting. We demonstrate our improvement discussed in Sects. 4 and 6 by comparing with [16]. First, we note that in [16], (i) the face-normal tetrisation, (ii) the error function E_T, (iii) and the blending function Blend_P are used. We

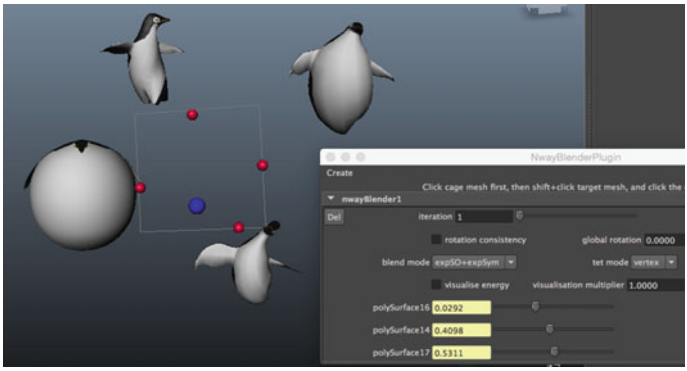

Fig. 8 Our Maya plugin

have already seen the difference between the blending functions Blend_P and Blend_C at the end of Sect. 5. We will turn our attention to (i) and (ii). Figure 9 visually compares different tetrisations in Sect. 4 and the error functions E_T and E_S in Sect. 6. We observe that E_S produces more natural results than E_T but much slower as we see in Table 1. With E_S, the face-normal tetrisation causes extra wrinkles compared to the edge-normal and the vertex-normal tetrisations. As far as we experimented, it depends on the character of shapes to be blended which tetrisation gives the best result. In general, with E_T the output is more or less similar regardless of the choice of tetrisation. With E_S, the vertex-normal tetrisation seems to be a good choice.

Table 1 shows a timing comparison for different tetrisations and error functions. We blended two 3D models each with 26 k triangles on a Macbook Air with 1.7 GHz Intel Core i7 and 8 GB memory. Initialisation part involves the Cholesky decomposition of the space matrix necessary to solve the minimiser of the error functions. This is computed only once in the initialisation process. Note that the matrix is dependent on the tetrahedral structure but independent of the choice of the error function. Runtime part consists of finding the minimiser of the error functions and the computation of Blend functions.

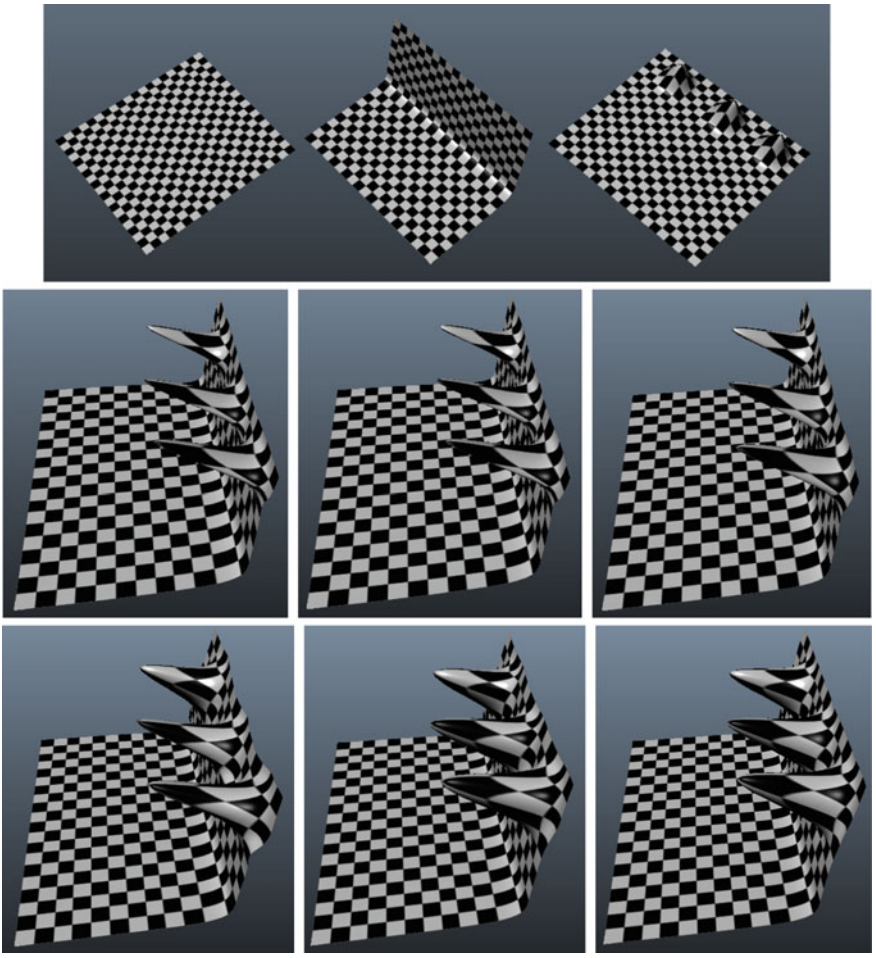

Fig. 9 *Top row* from *left* to *right* rest shape V_0 and its two deformations V_1 and V_2 to be blended with weights $w_1 = 1.0$ and $w_2 = 1.5$. *Second row* from *left* to *right* results obtained by face-normal, edge-normal, and vertex-normal tetrisation with E_T. *Third row* same as the second row but with E_S

Table 1 Timing comparison

	Face E_T	Edge E_T	Vertex E_T	Face E_S	Edge E_S	Vertex E_S
Initialisation (s)	0.1976	0.3080	0.3556	0.1976	0.3080	0.3556
Runtime with Blend$_P$	45.45 fps	27.43 fps	30.86 fps	11.66 fps	4.132 fps	4.762 fps
Runtime with Blend$_C$	48.46 fps	29.31 fps	31.46 fps	12.19 fps	4.576 fps	5.037 fps

Acknowledgments This work was partially supported by the Core Research for Evolutional Science and Technology (CREST) Program titled "Mathematics for Computer Graphics" of the Japan Science and Technology Agency (JST), by KAKENHI Grant-in-Aid for Young Scientists (B) 26800043, and by JSPS Postdoctoral Fellowships for Research Abroad.

References

1. M. Alexa, D. Cohen-Or, D. Levin, As-Rigid-As-Possible Shape Interpolation. Proc. ACM SIGGRAPH **2000**, 157–164 (2000)
2. W. Baxter, P. Barla, K. Anjyo, N-way morphing for 2D animation. Comput. Anim. Virtual Worlds **20**(2–3), 79–87 (2009)
3. M. Botsch, O. Sorkine, On linear variational surface deformation methods. IEEE Trans. Vis. Comput. Gr. **14**(1), 213–230 (2008)
4. M.S. Floater, Mean value coordinates. Comput. Aided Geom. Des. **20**(1), 19–27 (2003)
5. N. Higham, Computing the polar decomposition-with applications. SIAM J. Sci. Stat. Comput. **7**(4), 1160–1174 (1986)
6. S. Kaji, An N-way morphing plugin for Autodesk Maya, https://github.com/shizuo-kaji/NWayBlenderMaya
7. S. Kaji, G. Liu, Probe-type deformers, in *Mathematical Progress in Expressive Image Synthesis II* (Springer, Japan, 2015), pp. 63–77
8. S. Kaji, H. Ochiai, A concise parametrisation of affine transformation, preprint arXiv:1507.05290
9. L. Kavan, S. Collins, J. Žára, C. O'Sullivan, Geometric skinning with approximate dual quaternion blending. ACM Trans. Gr. **27**(4), 105:1–105:23 (2008)
10. Y. Lipman, O. Sorkine, D. Levin, D. Cohen-Or, Linear rotation-invariant coordinates for meshes. ACM Trans. Gr. **24**(3), 479–487 (2005)
11. K. Shoemake, Animating rotation with quaternion curves. ACM SIGGRAPH (1985), pp. 245–254
12. K. Shoemake, T. Duff, Matrix animation and polar decomposition, in *Proceedings of Graphics interface '92*, ed. by K.S. Booth, A. Fournier (Morgan Kaufmann Publishers Inc., San Francisco, 1992), pp. 258–264
13. H. Si, TetGen, a Delaunay-based quality tetrahedral mesh generator. ACM Trans. Math. Softw. **41**(2), 11:1–11:36 (2015)
14. O. Sorkine, M. Alexa, As-rigid-as-possible surface modeling, in *Proceedings of Eurographics SGP '07, Eurographics Association, Aire-la-Ville, Switzerland* (2007), pp. 109–116
15. R.W. Sumner, J. Popović, Deformation transfer for triangle meshes. ACM Trans. Gr. **23**(3), 399–405 (2004)
16. R.W. Sumner, M. Zwicker, C. Gotsman, J. Popović, Mesh-based inverse kinematics. ACM Trans. Gr. **24**(3), 488–495 (2005)
17. Y. Yu, K. Zhou, D. Xu, X. Shi, H. Bao, B. Guo, H.-Y. Shum, Mesh editing with poisson-based gradient field manipulation. ACM Trans. Gr. **23**(3), 644–651 (2004)

http://www.springer.com/978-981-10-1075-0

Mathematical Progress in Expressive Image Synthesis III
Selected and Extended Results from the Symposium MEIS2015
Dobashi, Y.; Ochiai, H. (Eds.)
2016, XII, 152 p. 78 illus., 64 illus. in color., Hardcover
ISBN: 978-981-10-1075-0